Eur. Phys. J. B **53**, 199–203 (2006)
DOI: 10.1140/epjb/e2006-00358-7

THE EUROPEAN PHYSICAL JOURNAL B

Vortex pinning in superconducting Nb thin films deposited on nanoporous alumina templates

W. Vinckx[1,a], J. Vanacken[1], V.V. Moshchalkov[1], S. Mátéfi-Tempfli[2], M. Mátéfi-Tempfli[2], S. Michotte[2], and L. Piraux[2]

[1] INPAC - Institute for Nanoscale Physics and Chemistry, Nanoscale Superconductivity and Magnetism & Pulsed Fields Group, K.U. Leuven, Celestijnenlaan 200D, 3001 Leuven, Belgium
[2] Unité de Physico-Chimie et de Physique des Matériaux (PCPM), Université Catholique de Louvain, Place Croix du Sud 1, 1348 Louvain-la-Neuve, Belgium

Received 17 July 2006 / Received in final form 31 August 2006
Published online 4 October 2006 –

Abstract. We present a study of magnetization and transport properties of superconducting Nb thin films deposited on nanoporous aluminium oxide templates. Periodic oscillations in the critical temperature vs. field, matching effects in fields up to 700 mT and strongly enhanced critical currents were observed. These fields are considerably higher than those typical for periodic pinning arrays made by lithographic techniques, which reflects the benefits of nanostructuring superconductors by using self-organized growth. This method provides a periodic pinning potential with sub-100 nm spacing between the pinning centers, which enhances vortex pinning in broad field and temperature ranges.

PACS. 74.25.Qt Vortex lattices, flux pinning, flux creep – 74.78.Na Mesoscopic and nanoscale systems

1 Introduction

During the last decade a considerable amount of work has been performed to improve the critical parameters of superconductors. It has been demonstrated in extenso that through the process of quantum design [1], i.e. by controlling the quantization effects through lateral nanomodulation with a characteristic length comparable with relevant length scales of the superconductor such as the coherence length $\xi(T)$ and the penetration depth $\lambda(T)$, its phase diagram can be significantly altered. More specifically, the introduction of periodic arrays of well-defined pinning centers such as holes (antidots) [2], blind holes [3], and ferromagnetic dots [4] can enhance the vortex pinning and reduce flux flow in superconducting thin films, thus giving rise to higher critical currents. Lithographically prepared arrays of pinning centers provide a model system to manipulate vortex patterns by incorporating a periodic pinning potential giving rise to several new static and dynamical vortex phases. Apart from precise control over the flux pinning properties, direct and precise manipulation of flux flow has been achieved recently through nanoengineered vortex ratchets [5] using periodic arrays of antidots with a built-in asymmetry, providing an asymmetric pinning potential for vortices. Nevertheless, the majority of these phenomena take place at relatively low fields (∼20 G) and close to the critical temperature of low-T_c superconductors, thus restricting their use in practical high-field applications. In addition, these nanostructured superconductors mentioned are usually fabricated using serial and time-consuming methods such as e-beam lithography.

In this paper we will focus on an alternative method to grow large arrays of holes, namely self-organized growth. Nowadays, the use of self-assembled templates attracts much attention because of their versatility, parallel processing, and potential low-cost (for an overview, see Xia et al. [6] and references herein). Furthermore, the *bottom-up* approach of self-assembled materials in contrast to the *top-down* lithographic approach has certain advantages in the sense that the modulation length achieved can be smaller than typical lithographic dimensions by more than one order [6]. We have already shown in a previous work that a modulating surface of polystyrene colloid nanospheres can increase the first matching field H_1 by one order of magnitude compared to $H_1 \sim 10$ G for lithographic arrays [7].

The template used in this work is anodized aluminium oxide grown from Al on a Si substrate by a carefully controlled electrochemical oxidation of Al [8,9]. Anodic Al_2O_3 has already proven its value for the growth of metallic [10], semiconducting [11] and magnetic nanowires [12] or as a commercially available nanoporous filter. The Al_2O_3 template is basically a several micron thick membrane-like structure consisting of a triangular array of parallel pores. In our case, the mean diameter of the pores is 40 nm and the interpore distance is about 100 nm. Thin Nb films were grown on these anodized alumina templates, inheriting their periodic membrane structure.

[a] e-mail: wim.vinckx@fys.kuleuven.be

Welp et al. demonstrated that the membrane structure of anodized aluminium foils can provide a periodic pinning potential in superconductors [13]. In this paper we use porous membranes directly grown on Si and provide detailed information about pinning properties of superconducting Nb films directly deposited on these membranes by measuring magnetization and electric transport on bridge shaped samples. Niobium films are type-II superconductors (SC) with Ginzburg-Landau (GL) parameter $\kappa = \lambda/\xi > 1/\sqrt{2}$, where λ and ξ are the penetration depth and the coherence length, $\lambda(T) = \lambda(0)/\sqrt{1-T/T_c}$ and $\xi(T) = \xi(0)/\sqrt{1-T/T_c}$ and T_c is the critical temperature of the superconductor. We show that the high density triangular array of nanopores provides a periodic pinning potential for vortices in the superconducting Nb film. This will result in the appearance of matching effects up to 700 mT and enhanced critical currents persisting down to temperatures as low as $0.7T_c$ due to a small interpore spacing.

2 Experimental

The supported nanoporous alumina template used in this work was prepared by electrochemical oxidation of a 5 μm thick aluminium layer evaporated onto a Si substrate. Anodic oxidation of the Al layer was performed in 0.3 M oxalic acid at 2 °C under a constant voltage of 40 V giving a mean interpore distance of about 100 nm. A two step anodization method was chosen where the first step was conducted for a depth of 4 μm in the Al layer in order to enhance the ordering of the pores. After a selective removal of the previously formed oxide layer using a mixture of 6 wt% H_3PO_4: 1.8 wt% chromic acid at 60 °C, a second anodization step was applied to form ordered arrays of nanopores on the substrate. Then, by chemical widening with a solution of 5 wt% H_3PO_4 at 30 °C, the diameter of the pores was adjusted to about half of the mean interpore distance. Thin Nb films were deposited on top of the alumina templates using molecular beam epitaxy (MBE) at room temperature with a working pressure of $\sim 10^{-10}$ Torr and an evaporation rate of 1.4×10^{-10} m/s. Reference films were grown in the same run on SiO_2 substrates. These films were checked with low angle XRD (X-ray diffraction), yielding a thickness of 50 nm. The surface of the substrates was investigated with SEM (Scanning Electron Microscopy) before and after deposition. Transport measurements were carried out in a PPMS cryostat (Quantum Design) by applying a four-probe ac-technique with an ac-current of 10 μA at 19 Hz, on samples evaporated through a mask in the shape of a transport bridge (width 200 μm, 2 mm distance between voltage contacts). The samples were electrically connected by ultrasonic wedge bonding. Magnetization measurements were carried out on $\sim$6 mm^2 samples using a VSM apparatus (vibrating sample magnetometer, Oxford Instruments) with a typical sweep rate of 0.06 T/min and a temperature stability close to 20 mK. The magnetic field was applied perpendicularly to the sample surface in both measurement types.

3 Results and discussion

Figure 1 displays SEM images of the anodized aluminium oxide (AAO) sample covered with Nb (hereafter referred to as AAO/Nb), (a) after the anodization of the Al/Si substrate (b) zooming-in on a small portion of (a) and, (c) after the deposition of Nb on the porous structure. Figures 1a and 1b show the AAO substrate, possessing a triangular array of period $d = 100$ nm of pores with diameter $D = 40$ nm. Figure 1c shows that the alumina periodical structure is transposed to the superconductor upon growth, which results in a high-density array of pores acting as holes in the Nb film, consisting of well-ordered domains of μm size. The first matching field H_1 for such ordered arrays can then be calculated to be $H_1 = 2\phi_0/\sqrt{3}d^2 = 232.8mT$.

The critical temperatures of the bridge shaped samples were determined using a resistance criterium $R_{crit} = 50\%$ R_n, R_n being the normal state resistance in zero applied field before the transition sets in.We found $T_c = 8.202$ K and 7.082 K for the reference film and the AAO/Nb sample, respectively. We suspect this discrepancy to have its origin in the proximity effect with aluminium at the AAO/Nb interface, and by contamination of the AAO surface during anodisation and/or the roughness of the AAO surface compared to the flat SiO_2 substrate.

The $T_c(H)$ phase boundary was extracted from a series of field cooled $R(T)$ (resistance vs. temperature) measurements. Figure 2 shows the phase diagram of both samples. One can immediately see that the introduction of the dense hole array provided by the alumina template strongly modifies the superconducting phase of a plain Nb thin film if the difference in critical temperature is disregarded. The reference bridge shows the expected linear phase boundary of a plain film. The dashed line extrapolates the data to higher fields in order to compare with the hole array sample. A fit of the data with the expression $H_{c2}(T) = \phi_0/2\pi\xi^2(T)$, yields a value of $\xi(0) \approx 7$ nm. In the case of the AAO/Nb sample, one observes periodic anomalies superimposed on a parabolic background crossing over to a linear background at lower temperatures. A pronounced bump around $H/H_1 = 1$ and a weak shoulder at the second matching field $H/H_1 = 2$ are seen. To improve the visualization of the periodic anomalies present, the insert of Figure 2 shows the $R(T)$ transition width as a function of field, in which matching features should become visible as local transition width minima. The two anomalies at $H/H_1 = 1$ and 2 are well reproduced, while two additional shallow minima are revealed at reduced field values coinciding with $H/H_1 = 3$ and 4. These resistance minima occur at multiples of the field value of 220 mT, which is in good agreement with the calculated value of $H_1 = 232.8$ mT. At this point, there is no indication of rational matching effects. The particular vortex lattice configurations at the matching fields will be discussed later.

The parabolic behavior of the $T_c(H)$ phase boundary modulated by periodic anomalies is reminiscent of the work conducted on superconducting wire networks [14] and perforated superconducting thin films [15]. At

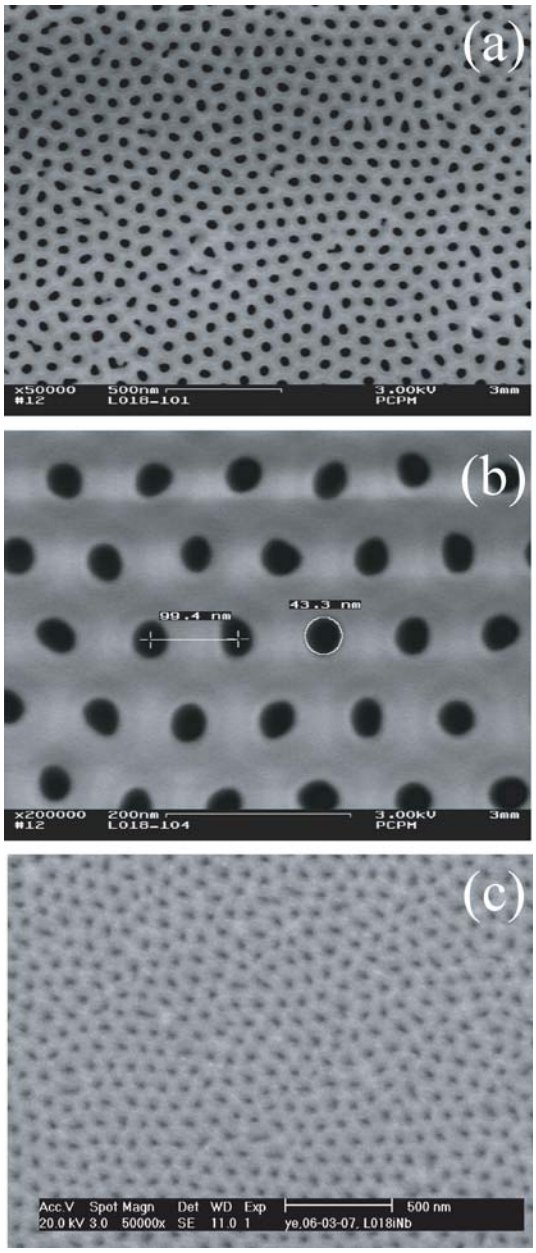

Fig. 1. SEM-image of (a) the anodised aluminium oxide substrate, (b) zooming-in on individual pores with indication of interpore distance and pore diameter, and (c) the aluminium oxide substrate covered with 50 nm Nb. Notice the Nb porous structure inherited from the virgin substrate. The length scales are indicated.

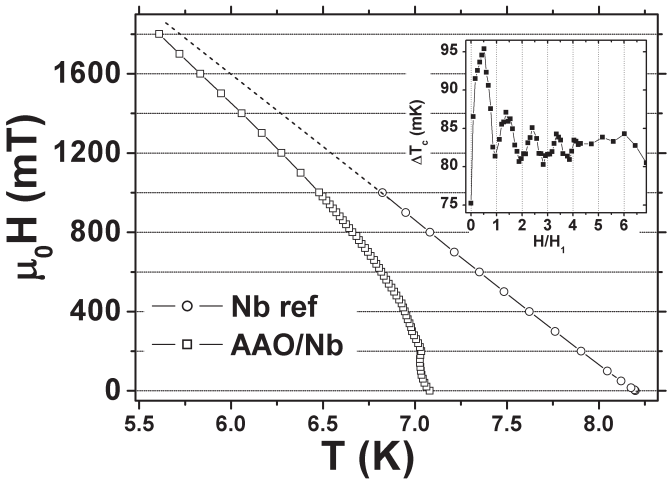

Fig. 2. $Tc(H)$ phase boundary determined from field cooled resistance vs. temperature curves. The horizontal axis indicates the temperature and the vertical axis represents the applied magnetic field. The dashed line extrapolates the low-field data for the reference film to higher fields for comparison. The inset shows the resistance vs. temperature $R(T)$ transition width $\Delta T_c(H) = T_c(\mathrm{R_{crit}} = 75\%R_n) - T_c(\mathrm{R_{crit}} = 25\%R_n)$ of the AAO/Nb sample in function of the calculated value for the first matching field $H_1 = 232.8$ mT.

temperatures close to T_c the Nb array acts basically as a superconducting wire network: the parabolic background can be interpreted as originating [16] from superconducting stripes of width w between the holes, when $w \leq \xi(T)$. The periodic anomalies can then be regarded as fluxoid quantization effects in a multiply connected geometry [17]. The phase boundary of a stripe of width w is given [18] by $H_{c2}(T) = \sqrt{12}\phi_0/2\pi w\xi(T)$. The width of the stripes between the holes is calculated from SEM-data to be $w \approx 55$ nm. A fit of the data yields a value of $\xi(0) \approx 7$ nm. The same value of $\xi(0)$ is actually obtained when fitting the linear low temperature data ($<0.9T_c$) with the expression $H_{c2}(T) = \phi_0/2\pi\xi^2(T)$. So, both reference and AAO/Nb sample are in the dirty limit regime [19] with an electron mean free path $l = 1.38\xi^2(0)/\xi_0 \approx 2$ nm, with $\xi_0 = 39$ nm the BCS-coherence length of Nb [20]. From this value and the value of the London - penetration depth for Nb, $\lambda_L = 39$ nm, the penetration depth can be calculated to yield $\lambda(0) = 0.66\lambda_L\sqrt{\xi_0/l} \approx 114$ nm. However, the multiply connected AAO structure allows the magnetic field to penetrate more easily into the superconducting Nb film and the penetration depth $\lambda(0)$ should then be modified [21] and replaced by an effective penetration depth $\Lambda(0) = \lambda(0)/\sqrt{1 - 2S_A/S_t} = 204$ nm, with S_A and S_t the area occupied by the antidots and the total area, respectively. Ultimately, we can conclude that the AAO template induces a periodic pinning potential in the Nb thin film ($\xi_0/d \approx 0.1$) capable of dominating vortex pinning in a relatively broad temperature range ($\Lambda(0)/d \approx 2$).

Vibrating Sample Magnetometer (VSM) measurements were carried out at several temperatures. The critical temperature of reference and hole sample was measured in a SQUID - magnetometer to be 8.92 K and 8.12 K, respectively. Figure 3 shows magnetization loops for both films at different temperatures. The strongly enhanced pinning of vortices in the antidot array compared to the reference is clearly established. In contrast to previous studies on lithographic antidot arrays, matching effects up to $H/H_1 = 3$ remain present at low temperatures. Only at temperatures below $0.7T_c$ intrinsic

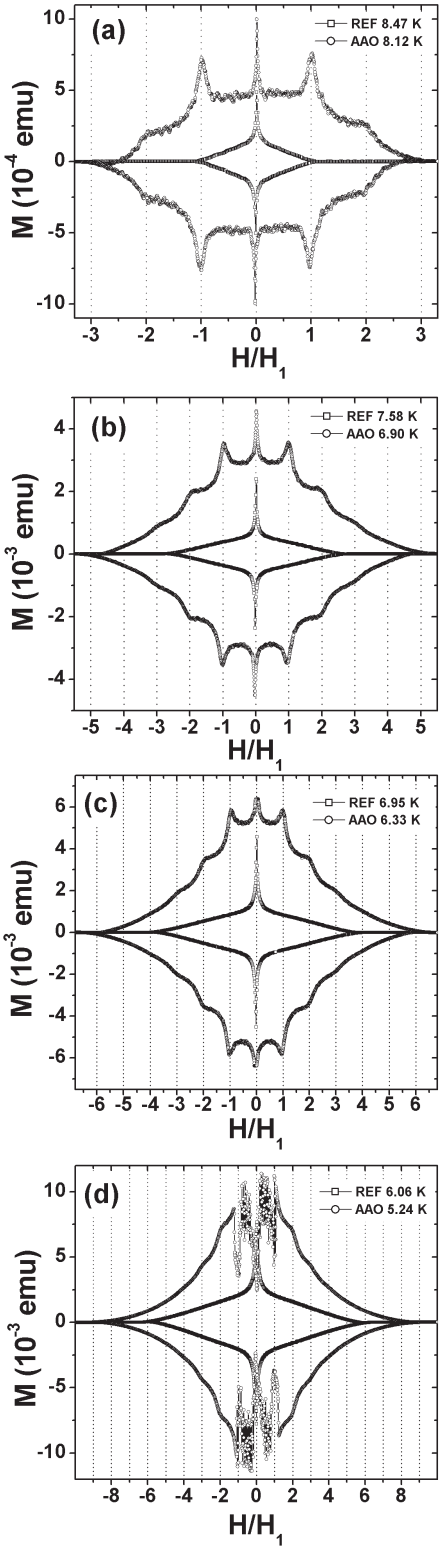

Fig. 3. VSM magnetisation curves at several reduced temperatures of the reference and the AAO/Nb sample, (a) $T/T_c = 0.95$, (b) $T/T_c = 0.85$, (c) $T/T_c = 0.78$, and (d) $T/T_c = 0.68$. The horizontal axis represents the external magnetic field in units of the first matching field ($H_1 = 232.8$ mT) for the AAO/Nb structure. Open circles and squares represent the AAO/Nb array and the reference film, respectively. They have both the same area ($\sim$6 mm^2) and the same thickness (50 nm).

pinning effects grow in strength, leading to strongly nonlinear magnetic behavior at fields below H_1, e.g. vortex avalanches [22] (see Fig. 3d). According the Bean critical state model [23], the critical current density j_c can be estimated directly from the magnetization width i.e. $j_c(H) \sim \Delta M(H) = M^+(H) - M^-(H)$, showing that j_c of the antidot sample has increased by almost two orders of magnitude compared to the reference sample in a wide field range at all temperatures.

The magnetization loops displayed in Figure 3 show a peak at the first matching field H_1 followed by a monotonous drop to zero, interrupted by shoulder-like behavior at $H/H_1 = 2$ and 3. This can be explained by the fact that the antidots are able to trap only a single quantized vortex (ϕ_0) before saturation sets in and composite vortex lattices of defect pinned single quantized vortices and interstitial single quantized vortices are formed [24]. The saturation number n_s of the antidots can be estimated using the criterion of Mkrtchyan and Shmidt [25] for an isolated cylindrical cavity, which is $n_s = D/4\xi(T)$ with D the diameter of the antidot. This criterium yields $n_s \approx 1$ for our sample at all temperatures. Neither are double quantized ($2\phi_0$) vortices likely to be pinned by the antidots. This can be estimated using the criterium put forward by Buzdin [26], stating that a triangular vortex lattice of ($2\phi_0$) vortices would only be energetically stable when $D > \sqrt[3]{8\xi(T)d^2}$, where the minimally allowed diameter size would be $D \geq 63$ nm (at $T = 0$) which is clearly not fulfilled in our case.

In fields higher than the first matching field, when every antidot is occupied by a single quantized vortex, vortices will occupy positions between the antidots. These interstitial vortices experience a caging potential originating from the strongly pinned vortices at the antidots. The strength of the caging potential is governed by the vortex-vortex interactions i.e. the number of vortices and the ratio $\lambda(T)/d$. We have deduced from transport measurements in a previous paragraph that $\Lambda(0)/d \approx 2$, which allows the caging potential to remain periodic even at low temperatures. This results in the appearance of matching effects up to $H = 3H_1$ with a periodic composite vortex lattice configuration shown in Figure 4. As the magnetic field increases, the number of vortices present in the sample grows and individual vortex-vortex interactions become important: the periodic caging lattice is gradually destabilized and matching effects at higher fields are being suppressed.

The specific vortex lattice configurations stabilized at matching fields $\{H_1, H_2, H_3\}$ are shown in Figure 4. In the case of $H/H_1 = 1$ a commensurate triangular vortex lattice is formed, while a vortex lattice with hexagonal symmetry can be formed at $H/H_1 = 2$. At $H/H_1 = 3$ a composite triangular vortex lattice can be formed. Transport or magnetization measurements did not show any indication of the existence of rational matching effects, which can be attributed to the strong vortex-vortex interaction due to the enhanced penetration depth $\Lambda(T)$ forcing the vortices to be pinned at the antidots, and the lack of large-scale order in the Nb arrays.

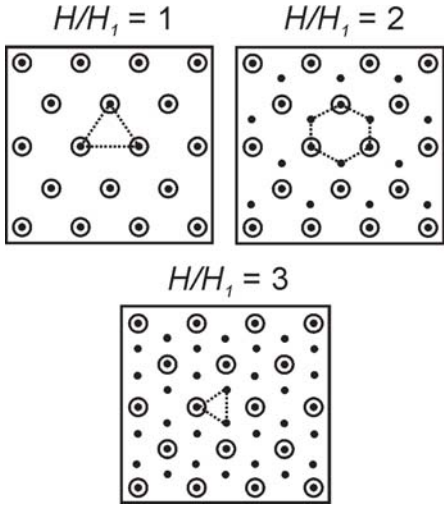

Fig. 4. Schematic presentation of the vortex configurations present in the Nb hole array. Open circles and black dots represent the holes and vortices, respectively. The dotted figures represent the unit cell of the vortex lattice.

4 Conclusions

We have grown large scale superconducting antidot arrays from Si supported anodized alumina substrates. Transport and magnetization measurements have established the existence of pronounced matching effects up to 700 mT at temperatures as low as 5.7 K. The critical current density was shown to be increased by two orders of magnitude. The unique characteristic of the anodic alumina nanotemplate is in the fact that it provides a periodic pinning potential which works well also at lower temperatures, through a combination of the enhancement of the penetration depth and the sub-100 nm defect spacing in the template. Future work will incorporate a regular array of magnetic Co nanowires grown inside the pores of alumina membranes with a superconductor on top, which is expected to provide a richer and more complex vortex pinning behavior due to the magnetic interaction between the nanowires and vortices.

This work was supported by the Belgian Science Policy through the Interuniversitary Attraction Pole Programme (IAP 5/1/1), the Flemish FWO and the Research fund KU Leuven GOA/2004/02 programmes as well as the ESF programme "AQDJJ" and the "Communauté Française de Belgique" through the Program "Actions de Recherches Concertées". S.M. is a postdoctoral researcher of the FNRS. W.V. would like to thank B. Opperdoes for the preparation of the Nb films, and D. Smeets for the xrd - measurements.

References

1. V.V. Moshchalkov, V. Bruyndoncx, L. Van Look, M.J. Van Bael, Y. Bruynseraede, in *Handbook of Nanostructured Materials and Nanotechnology*, edited by H.S. Nalwa (Academic Press, San Diego, 2000), **3**, Chap. 9
2. A.T. Fiory, A.F. Hebard, S. Somekh, Appl. Phys. Lett. **32**, 73 (1978); M. Baert, V.V. Metlushko, R. Jonckheere, V.V. Moshchalkov, Y. Bruynseraede, Phys. Rev. Lett. **74**, 3269 (1995)
3. S. Raedts, A.V. Silhanek, M.J. Van Bael, V.V. Moshchalkov, Phys. Rev. B **70**, 024509 (2004)
4. J.I. Martin, M. Velez, J. Nogues, I.K. Schuller, Phys. Rev. Lett. **79**, 1929 (1997); M. Lange, M.J. Van Bael, Y. Bruynseraede, V.V. Moshchalkov, Phys. Rev. Lett. **90**, 197006 (2003)
5. J. Van De Vondel, C.C. de Souza Silva, B.Y. Zhu, M. Morelle, V.V. Moshchalkov, Phys. Rev. Lett. **94**, 057003 (2005); C.C.D. Silva, J. Van De Vondel, M. Morelle, V.V. Moshchalkov, Nature (London) **440**, 7084 (2006)
6. Y.N. Xia, B. Gates, Y.D. Ying, Y. Lu, Adv. Mater. **12**, 693 (2000)
7. W. Vinckx, J. Vanacken, V.V. Moshchalkov, J. Appl. Phys. **100**, 044307 (2006)
8. J.P. O'Sullivan, G.C. Wood, Proc. R. Soc. London, Ser. A **317**, 511 (1970)
9. H. Masuda, K. Fukuda, Science **268**, 1466 (1995); O. Jessensky, F. Müller, U. Gösele, Appl. Phys. Lett. **72**, 1173 (1998)
10. G. Sauer, G. Brehm, S. Schneider, K. Nielsch, R.B. Wehrspohn, J. Choi, H. Hofmeister, U. Gösele, J. Appl. Phys. **91**, 3243 (2002)
11. Y. Li, G.W. Meng, L.D. Zhang, F. Phillipp, Appl. Phys. Lett. **76**, 2011 (2000)
12. J. Mallet, K. Yu-Zhang, S. Mátéfi-Tempfli, M. Mátéfi-Tempfli, L. Piraux, J. Phys. D **38**, 909 (2005)
13. U. Welp, Z.L. Xiao, J.S. Jiang, V.K. Vlasko-Vlasov, S.D. Bader, G.W. Crabtree, Phys. Rev. B **66**, 212507 (2002)
14. B. Pannetier, J. Chaussy, R. Rammal, J.C. Villegier, Phys. Rev. Lett. **53**, 1845 (1984)
15. A. Bezryadin, B. Pannetier, J. Low Temp. Phys. **98**, 251 (1995)
16. T. Puig, L. Van Look, M.J. Van Bael, V.V. Moshchalkov, Y. Bruynseraede, R. Jonckheere, Phys. Rev. B **58**, 5744 (1998)
17. R.D. Parks, W.A. Little, Phys. Rev. **133**, A97–A103 (1964)
18. M. Tinkham, *Introduction to Superconductivity* (McGraw-Hill, New York, 1975)
19. V.V. Schmidt, *The Physics of Superconductors*, edited by P. Müller and A.V. Ustinov (Springer, Berlin-Heidelberg, 1997)
20. W. Buckel, *Supraleitung*, 3rd edn. (Physik-Verlag, Weinheim, 1984)
21. A. Wahl, V. Hardy, J. Provost, Ch. Simon, A. Buzdin, Physica C **250**, 163 (1995)
22. A. Terentiev, D.B. Watkins, L.E. De Long, L.D. Cooley, D.J. Morgan, J.B. Ketterson, Phys. Rev. B **61**, R9249 (2000); S. Hébert, L. Van Look, L. Weckhuysen, V.V. Moshchalkov, Phys. Rev. B **67**, 224510 (2003)
23. C.P. Bean, Phys. Rev. Lett. **8**, 250 (1962)
24. V.V. Moshchalkov, M. Baert, V.V. Metlushko, E. Rosseel, M.J. Van Bael, K. Temst, R. Jonckheere, Y. Bruynseraede, Phys. Rev. B **54**, 7385 (1996)
25. G.S. Mkrtchyan, V.V. Shmidt, Sov. Phys. JETP **34**, 195 (1972)
26. A.I. Buzdin, Phys. Rev. B **47**, 11416 (1993)